ISSN 1346-5597

NII National Institute of Informatics

NII Technical Report Sep 2002

Boundary Element Simulation of Large Amplitude Standing Waves in Vessels

Kenji HAMANO, Sunao MURASHIGE and Ken HAYAMI

NII-2002-004E
Sep 2002

URL: http://www.nii.ac.jp/ Tokyo 101-8430, JAPAN +81-3-4212-2000 FAX: +81-3-3556-1916

Boundary Element Simulation of Large Amplitude Standing Waves in Vessels

Kenji HAMANO [a,b], Sunao MURASHIGE [c], Ken HAYAMI [d]

[a] *Department of Mathematical Engineering and Information Physics, Graduate School of Engineering, The University of Tokyo, 7-3-1 Hongo, Bunkyo-ku, Tokyo 113-0033, Japan*

[b] *Presently at: Second Research Center, Technical Research and Development Institute, Japan Defense Agency, 1-2-24 Ikejiri, Setagaya-ku, Tokyo 154-8511, Japan*

[c] *Department of Complexity Science and Engineering, Graduate School of Frontier Sciences, The University of Tokyo, 7-3-1 Hongo, Bunkyo-ku, Tokyo 113-0033, Japan*

[d] *Mathematical Informatics Research, Foundations of Informatics Research Division, National Institute of Informatics, 2-1-2 Hitotsubashi, Chiyoda-ku, Tokyo 101-8430, Japan*

Abstract

In this paper, a fluid in a vessel is considered and large amplitude standing waves (LASW) of the fluid are simulated directly using the boundary element method (BEM).

In the simulation, two problems come out. The first problem is that the energy of the LASW increases gradually when using double nodes at corners in the BEM. The second problem is that projection-like profiles appear near the point where the free surface meets the vessel wall when regridding is not used at each time step. These projection-like profiles are not physical and indicate numerical error, and cause the simulation to break down.

We found that the use of discontinuous elements solves the first problem, and the use of the "half shift method" solves the second problem.

In addition, a method called RIG for highly accurate simulation using regridding is proposed and verified.

Key words: boundary element method, large amplitude standing waves, direct simulation

Email addresses: hamano@jda-trdi.go.jp (Kenji HAMANO),

1 Introduction

The study of large amplitude standing waves (LASW) is required in various areas. For example, melted iron containers are carried on rails in ironworks. The containers may oscillate and melted iron may spill out of the containers. Besides, for launching a rocket successfully, it is important to analyze how a liquid fuel moves inside the tank due to the rocket's oscillation and how in turn that effects the rocket's movement. Moreover, it is important to study the motion of liquid in ships, when the ships oscillate due to ocean waves. If the liquid in the ships starts to resonate, the ship's oscillation increases rapidly and in the worst case, the ship will overturn.

[11] can be cited for the direct simulation of LASW using BEM. They assume periodic waves as in the formulation of [6]. They map the free surface to a closed curve in the complex plane using the assumption of periodicity. Then, they apply BEM to the closed curve in the complex plane.

Most papers which simulate the dynamics of liquids in a vessel using BEM have an interest in handling sloshing analysis, and few papers simulate LASW in a vessel using BEM. Moreover, those papers which address LASW assume periodicity in most cases, and in some cases, a vortex-sheet method is used instead of BEM [13]. On the other hand, in our paper, we are concerned with the direct application of BEM to a boundary of a fluid in a vessel in order to simulate LASW, and do not use periodicity. In principle, the results of our paper can be applied to general waves (transient waves, stationary waves, transient traveling waves) and waves of finite depth. The direct application of BEM to the boundary causes a corner problem, and the corner points become the peak of LASW. In this respect, our simulation is more difficult than [6][11].

The overview of this paper is as follows. In section 2, the settings of our simulation are explained. In section 3, the basic formulation is given. In section 4, simulation results on the comparison of using double nodes and using discontinuous elements, the simulation result using the half_shift method, and the simulation result with the vertical excitation are presented. In section 5, the RIG algorithm for the highly accurate simulation is explained and verified. The simulation result with the vertical excitation using RIG is also shown. In section 6, the large amplitude cosine wave is simulated in order to show that our method can also simulate transient standing waves.

sunao@sat.t.u-tokyo.ac.jp (Sunao MURASHIGE), hayami@nii.ac.jp (Ken HAYAMI).

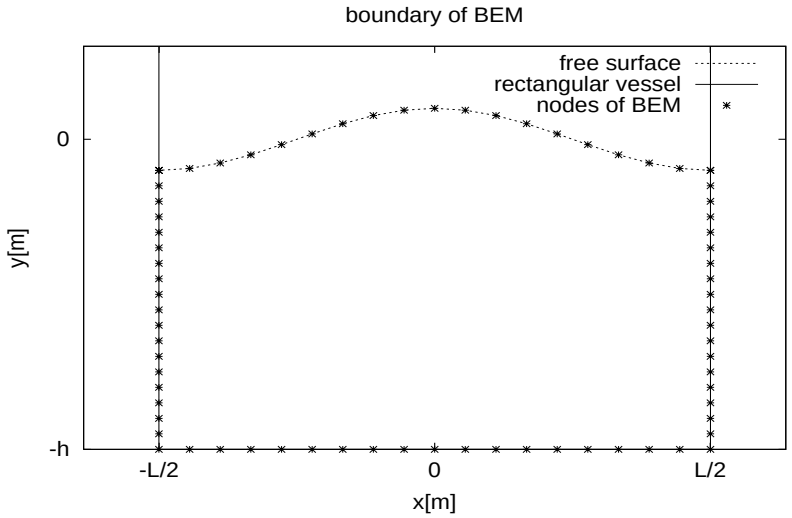

Fig. 1. Schematic illustration of the simulation.

2 Settings

A perfect fluid contained in a rectangular vessel in two dimensional space is considered (Fig. 1). We take the x-axis in the horizontal direction and the y-axis in the vertical direction. The fluid at surface in contact with air is called the free surface. The center of the vessel is $x = 0$[m], the width of the vessel is $L = 2\pi$[m], the distance between the bottom of the vessel and the still water surface ($y = 0$[m]) is $h \geq \dfrac{L}{2}$. Time is denoted by t[s], the displacement of the free surface from the still water surface is $\eta = \eta(x, t)$[m]. The bottom of the vessel is at $y = -h$[m], and the height of the vessel is $+\infty$[m]. The gravitational acceleration is $g = 9.8$[m/s^2]. The initial wave profile of our simulation is as shown in Fig. 1.

3 The numerical simulation method

3.1 The basic formulation

We consider an incompressible irrotational flow. The velocity potential ϕ can be defined. The velocity potential satisfies the Laplace's equation,

$$\Delta\phi = 0. \tag{1}$$

The velocity of fluid particles $(u, v)^{\mathrm{T}}$ satisfies the following equations,

$$u = \frac{\partial \phi}{\partial x}, \tag{2}$$

$$v = \frac{\partial \phi}{\partial y}. \tag{3}$$

$(u, v)^{\mathrm{T}}$ is also given by the following equations,

$$u = \frac{\mathrm{D}x}{\mathrm{D}t}, \tag{4}$$

$$v = \frac{\mathrm{D}y}{\mathrm{D}t}, \tag{5}$$

where $\dfrac{\mathrm{D}}{\mathrm{D}t}$ is the material derivative.

Positions of fluid particles on the free surface $(x, y)^{\mathrm{T}}$ satisfy the following equations,

$$\frac{\mathrm{D}x}{\mathrm{D}t} = \frac{\partial \phi}{\partial x}, \tag{6}$$

$$\frac{\mathrm{D}y}{\mathrm{D}t} = \frac{\partial \phi}{\partial y}. \tag{7}$$

From Bernoulli's equation, the velocity potential satisfies the following equation at the free surface,

$$\frac{\mathrm{D}\phi}{\mathrm{D}t} = \frac{1}{2}\left\{\left(\frac{\partial \phi}{\partial x}\right)^2 + \left(\frac{\partial \phi}{\partial y}\right)^2\right\} - g\eta. \tag{8}$$

Using the above evolution equations (6), (7) and (8), the time evolution of the free surface is simulated. $\dfrac{\partial \phi}{\partial x}, \dfrac{\partial \phi}{\partial y}$ can be calculated using BEM as the velocity potential ϕ satisfies the Laplace's equation. In this paper, the time evolution scheme based on the following Taylor expansion [8] was used.

$$x^{t+\Delta t} \approx x^t + \Delta t \frac{\mathrm{D}x}{\mathrm{D}t} + \frac{(\Delta t)^2}{2}\frac{\mathrm{D}^2 x}{\mathrm{D}t^2} + \frac{(\Delta t)^3}{3!}\frac{\mathrm{D}^3 x}{\mathrm{D}t^3} + \frac{(\Delta t)^4}{4!}\frac{\mathrm{D}^4 x}{\mathrm{D}t^4}. \tag{9}$$

$y^{t+\Delta t}$ and $\phi^{t+\Delta t}$ are expanded similarly. The second-order Lagrangian derivative is expressed as

$$\frac{\mathrm{D}^2 x}{\mathrm{D}t^2} = \frac{\partial \phi_t}{\partial x} + u\frac{\partial u}{\partial x} + v\frac{\partial u}{\partial y}, \tag{10}$$

where $\phi_t = \dfrac{\partial \phi}{\partial t}$. ϕ_t is also computed using BEM, since ϕ_t satisfies the Laplace's equation: $\Delta \phi_t = 0$, and the boundary values that $\phi_t = \dfrac{\mathrm{D}\phi}{\mathrm{D}t} - \left(u^2 + v^2\right)$ on the free surface and $\dfrac{\partial \phi_t}{\partial n} = 0$ on the bottom and the wall of the vessel can be obtained. Higher order derivatives of ϕ with respect to t are computed using BEM similarly.

3.2 BEM

In this part, we briefly explain the BEM [3] formulation.

Let Γ_f be the free surface, Γ_w be the boundary where the fluid contacts with the vessel. $\Gamma = \Gamma_f \cup \Gamma_w$ is a closed curve. Let Ω be the domain inside Γ.

The boundary integral equation (BIE)

$$\frac{\theta}{2\pi}\phi + \int_\Gamma \phi \frac{\partial \phi^*}{\partial n}\mathrm{d}\Gamma = \int_\Gamma \frac{\partial \phi}{\partial n}\phi^* \mathrm{d}\Gamma, \tag{11}$$

holds, where θ is the angle subtending Ω at the point on the boundary Γ, and ϕ^* is the fundamental solution.

Then, Γ and $\phi, \dfrac{\partial \phi}{\partial n}$ on Γ are discretized using linear elements ($\Gamma = \cup_i \Gamma_i$). The boundary integral equation (BIE) for node k is,

$$\frac{\theta_k}{2\pi}\phi_k + \sum_{i=1}^{n} \int_{\Gamma_i} \phi \frac{\partial \phi^*}{\partial n}\mathrm{d}\Gamma = \sum_{i=1}^{n} \int_{\Gamma_i} \frac{\partial \phi}{\partial n}\phi^* \mathrm{d}\Gamma. \tag{12}$$

The BIE is then approximated by collocation. The integrations over each element are done analytically. When n nodes are placed on Γ, n equations are obtained. When values of either ϕ or $\dfrac{\partial \phi}{\partial n}$ are known at each node, unknown values of either ϕ or $\dfrac{\partial \phi}{\partial n}$ at each node are solved from the system of n equations because there are n unknown values.

3.2.1 The corner problem

At the intersection points between Γ_f and Γ_w, $\dfrac{\partial\phi}{\partial n}$ has two different values. Such points are called corner nodes. At corner nodes, $\dfrac{\partial\phi}{\partial n}$ is discontinuous and the linear interpolation of $\dfrac{\partial\phi}{\partial n}$ causes inaccuracy. Thus, special care must be taken for the discontinuity of $\dfrac{\partial\phi}{\partial n}$.

There are two basic methods for this in BEM. The first method is to use double nodes [5] and the second method is to use discontinuous elements [2].

The use of double nodes is as follows. The corner node where Γ_f and Γ_w meet is split into two nodes k, k', and the values of ϕ and $\dfrac{\partial\phi}{\partial n}$ at the two nodes are treated as independent quantities $\phi_k, \phi_{k'}, \left.\dfrac{\partial\phi}{\partial n}\right|_k$ and $\left.\dfrac{\partial\phi}{\partial n}\right|_{k'}$. Because two of $\phi_k, \phi_{k'}, \left.\dfrac{\partial\phi}{\partial n}\right|_k$ and $\left.\dfrac{\partial\phi}{\partial n}\right|_{k'}$ are known values and two of $\phi_k, \phi_{k'}, \left.\dfrac{\partial\phi}{\partial n}\right|_k$ and $\left.\dfrac{\partial\phi}{\partial n}\right|_{k'}$ are unknown values, another two equations,

$$\phi_k = \phi_{k'}, \tag{13}$$

$$\frac{1}{2}\phi_{k'} - \frac{\pi-\theta_k}{2\pi}\phi_k + \sum_{\substack{i=1\\ i\neq j\\ i\neq k}}^{n} \int_{\Gamma_i} \phi \frac{\partial\phi^*}{\partial n}\,\mathrm{d}\Gamma = \sum_{i=1}^{n} \int_{\Gamma_i} \frac{\partial\phi}{\partial n}\phi^*\mathrm{d}\Gamma, \tag{14}$$

are introduced, where Γ_j and Γ_k are the two elements of Γ adjacent to node k.

The use of discontinuous elements is as follows. The nodes for ϕ and $\dfrac{\partial\phi}{\partial n}$ which meet at the corner are shifted inside the two elements adjacent to the corner. ϕ and $\dfrac{\partial\phi}{\partial n}$ are represented by linear functions along the whole elements in terms of their nodal values and both of them are in principle discontinuous at the corner. In the present paper, when n_a is a node of ϕ and $\dfrac{\partial\phi}{\partial n}$ at the corner and n_b is a node next to n_a, n_a is shifted to the point dividing the interval $\overline{n_a n_b}$ by the ratio 1:3.

4 Simulation results

4.1 Use of double nodes vs. discontinuous elements

For the initial wave profile, the large amplitude stationary standing waves obtained by Dr. M. Okamura[9] was used. The crest acceleration of η normalized by g ($A_c = -\frac{1}{g}\frac{\mathrm{D}\phi_y}{\mathrm{D}t}$) is 0.85. 63 nodes were placed on Γ_f, and regridding was used at every time step.

The regridding procedure is as follows. Let the x, y coordinates and the velocity potential ϕ at node i at time t be x_i^t, y_i^t, ϕ_i^t $(i = 1, 2, \ldots, f)$, respectively, where f is the number of nodes on the free surface. Using the time evolution scheme, $x_i^{t+\Delta t}, y_i^{t+\Delta t}, \phi_i^{t+\Delta t}$ $(i = 1, 2, \ldots, f)$ are obtained. Then, $x_i^{t+\Delta t}, y_i^{t+\Delta t}$ $(i = 1, 2, \ldots, f)$ are interpolated using spline interpolation[10]. The y coordinate (y_i') of the interpolated curve at x_i^t $(i = 1, 2, \ldots, f)$ are obtained. Then, $x_i^{t+\Delta t}, y_i^{t+\Delta t}$ $(i = 1, 2, \ldots, f)$ are substituted by x_i^t, y_i' $(i = 1, 2, \ldots, f)$, respectively, and $\phi_i^{t+\Delta t}$ $(i = 1, 2, \ldots, f)$ are substituted by

$$\phi_i^t + \sum_{k=1}^{4} \frac{1}{k!} \left(\Delta t \frac{\partial}{\partial t} + \Delta y \frac{\partial}{\partial y} \right)^k \phi_i^t \quad (i = 1, 2, \ldots, f), \tag{15}$$

respectively, where $\Delta y = y_i' - y_i^t$. The point of the regridding is that the x coordinates on the free surface remain the same.

The time evolution of LASW is simulated. Fig. 2 shows the evolution of the total energy. Two cases are shown. Namely, the case using double nodes and the case using discontinuous elements for corners where the free surface meets the vessel wall. It is observed that LASW simulation using discontinuous elements is more stable than using double nodes.

Fig. 3 shows the magnified profile at the right end of the free surface. $\eta = \eta(x, t)$ is the displacement of the free surface from the still water surface. Three cases are shown. Namely, the case using double nodes, the case using discontinuous elements, and the case using the method of [6] (250 nodes were placed on Γ_f in this case). Note that when using the method of [6], there is no corner problem since it assumes periodicity. The effect of the corner nodes can be observed by comparing the three cases. It is observed that there is a little declination between the profile using double nodes and using the method of [6], whereas, the profile using discontinuous elements matches well with that using the method of [6].

As a result, we recommend that discontinuous elements should be used when

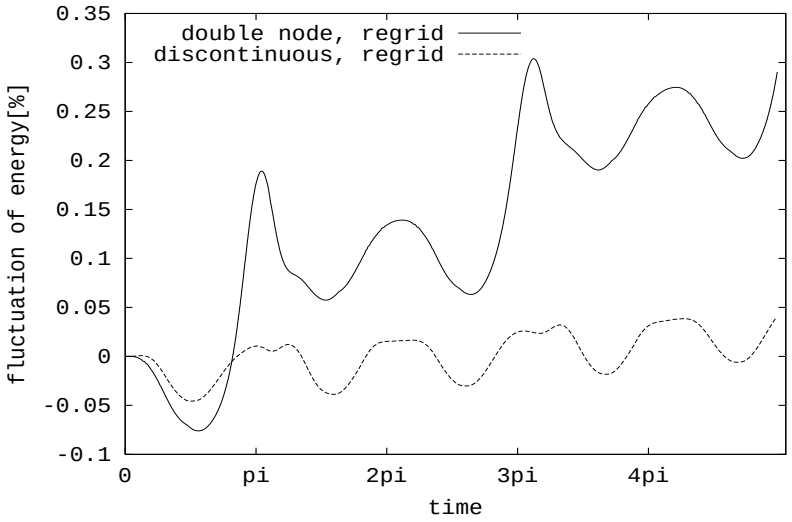

Fig. 2. Evolution of the total energy of the standing waves. Two cases are shown. Namely, the case using double nodes and regridding (double node, regrid) and the case using discontinuous elements and regridding (discontinuous, regrid).

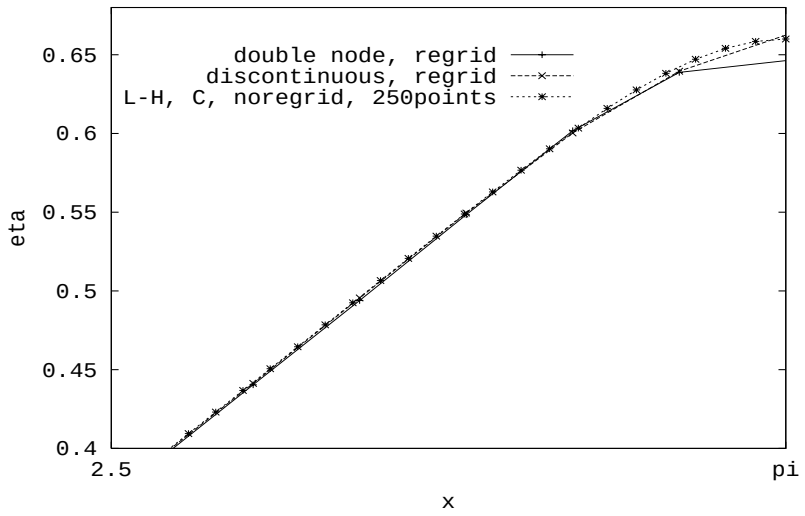

Fig. 3. Wave profiles for three cases: using double nodes and regridding (double node, regrid), using discontinuous elements and regridding (discontinuous, regrid) and using the method of [6] and without using regridding with 250 nodes on the free surface (L-H, C, noregrid, 250points).

simulating LASW with BEM.

4.2 The half shift method

Next, we consider the use of methods which can simulate LASW without using regridding. The reason considering this is that when the amplitude of

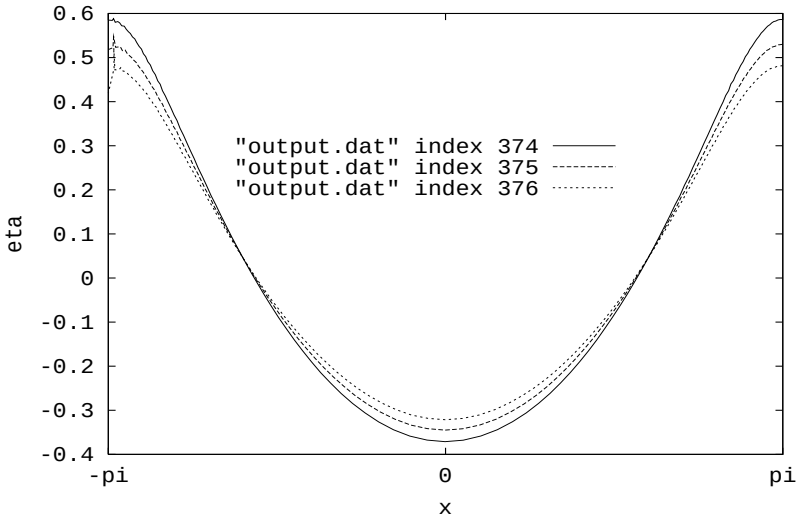

Fig. 4. Three wave profiles when the simulation without using regridding fails. Time progresses as the index number increases.

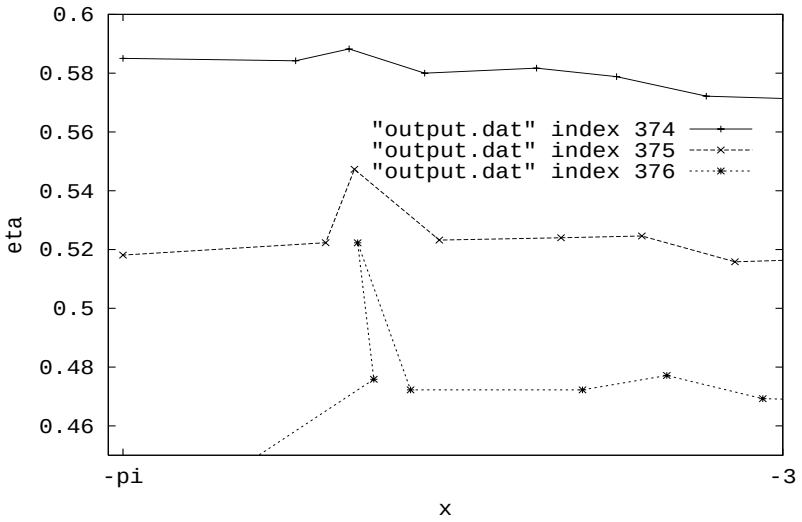

Fig. 5. Magnification of Fig. 4.

the standing waves become large, the accuracy of spline interpolation used in regridding may deteriorate, so that, if we want to simulate the limit amplitude standing waves, the simulation without using regridding may be required.

When the initial wave profile was set as Fig. 1, that is, when the center displacement of the free surface from the still water surface at $t = 0$: $\eta(0, 0)$ is at the highest and $\eta(\pi, 0), \eta(-\pi, 0)$ are at the lowest, and LASW is simulated without using regridding, projection-like profiles appear at the end of the free surface as shown in Fig. 4 and 5. These projection-like profiles are not physical and indicate numerical error, and that causes the simulation to break down.

Then, we consider two initial wave profiles. For the first profile, $\eta(0, 0)$ is at

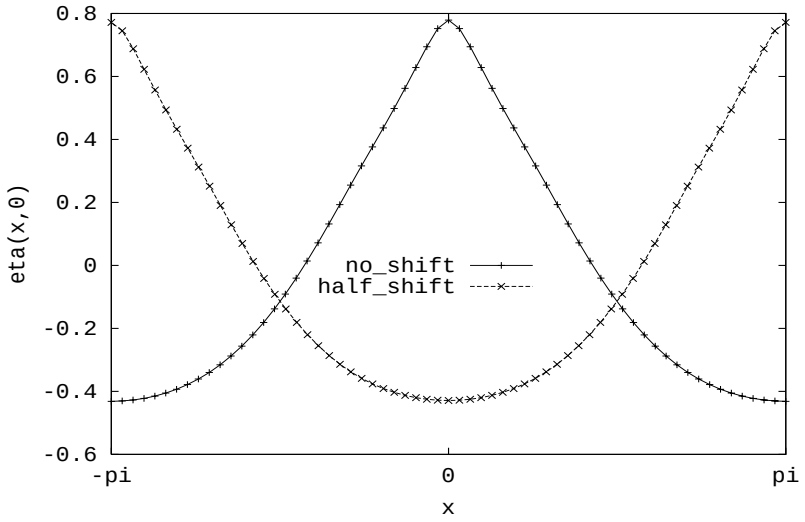

Fig. 6. The initial amplitude of the free surface $\eta(x, 0)$ ($A_c = 0.85$).

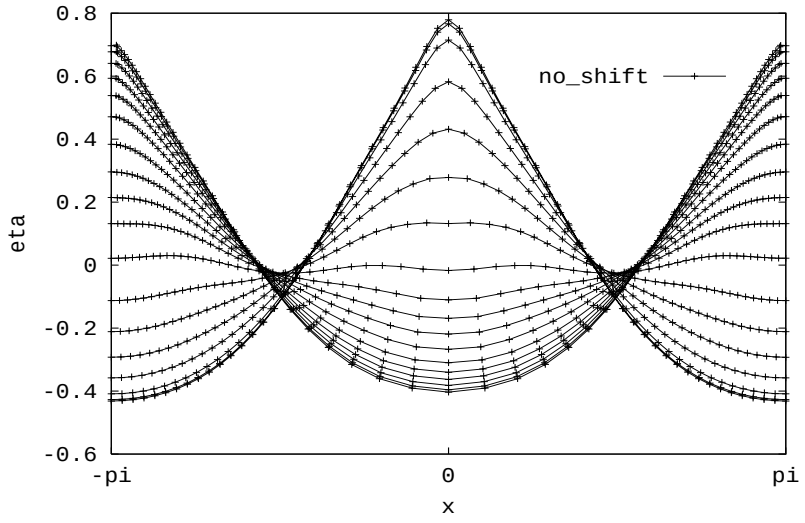

Fig. 7. Evolution of the wave profile. The initial amplitude of the free surface is set to no_shift of Fig. 6.

the highest and $\eta(\pi, 0), \eta(-\pi, 0)$ are at the lowest (no_shift), for the second, $\eta(0, 0)$ is at the lowest and $\eta(\pi, 0), \eta(-\pi, 0)$ are at the highest (half_shift) (see Fig. 6). In both cases, 63 nodes were placed on the free surface.

When the initial wave profile is set to no_shift of Fig. 6, the evolution of the free surface is as shown in Fig. 7. This simulation fails before half the period of oscillation, and nodes are found to concentrate towards the end of the free surface.

When the initial wave profile is set to half_shift of Fig. 6, the evolution of the free surface is as shown in Fig. 8. Different from the simulation of no_shift, this simulation does not fail, and the nodes do not concentrate towards the

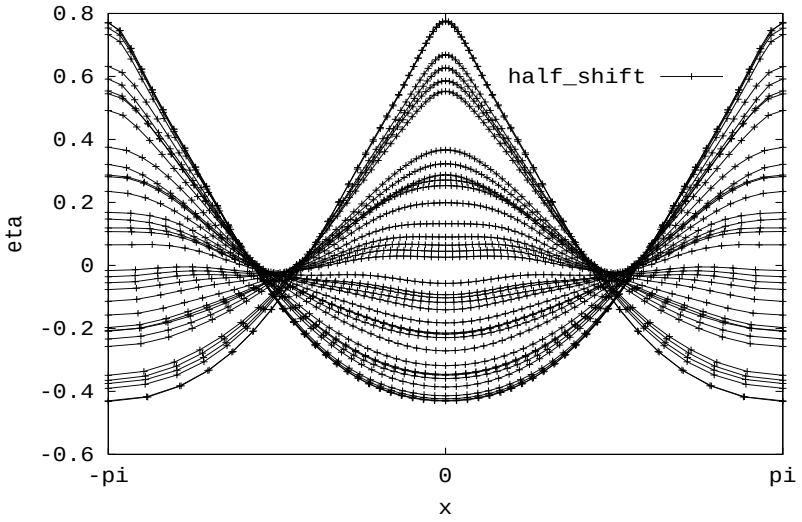

Fig. 8. Evolution of the wave profile. The initial amplitude of the free surface is set to half_shift of Fig. 6.

end of the free surface.

Therefore, shifting the initial wave profile by half the wave length prevents the concentration of nodes at the end of the free surface. This, in turn, enables us to avoid the formation of projection-like profiles, and renders the simulation without regridding feasible.

4.3 Simulation of excited standing waves

In this part, we excite the LASW with $A_c = -\frac{1}{g}\frac{\mathrm{D}\phi_y}{\mathrm{D}t} = 0.85$ in the vertical direction and make the LASW's amplitude larger and larger. The initial wave profile was set to the half_shift given in Fig. 6, and discontinuous elements were used. The oscillating amplitude was $d = 0.01$[m]. Since the depth of the vessel h is sufficiently large, the angular frequency ω of the free surface obtained from linear analysis is $\sqrt{g}$[1/s]. According to Mathieu's theory [1][7][13], when the angular frequency of the forced vertical oscillation is set to twice of ω, the amplitude of the standing waves becomes larger and larger. The oscillation is represented as follows:

$$g(t) = g + d(2\omega)^2 \sin(2\omega t)\ [\mathrm{m/s^2}]. \tag{16}$$

Fig. 9 shows the evolution of A_c, of the acceleration of $\eta(0,t)$ normalized by g, using regridding. Two cases are shown. Namely, the case when 127 nodes and 251 nodes were placed on the free surface, respectively. The results for both cases are clearly different and there are some disturbances.

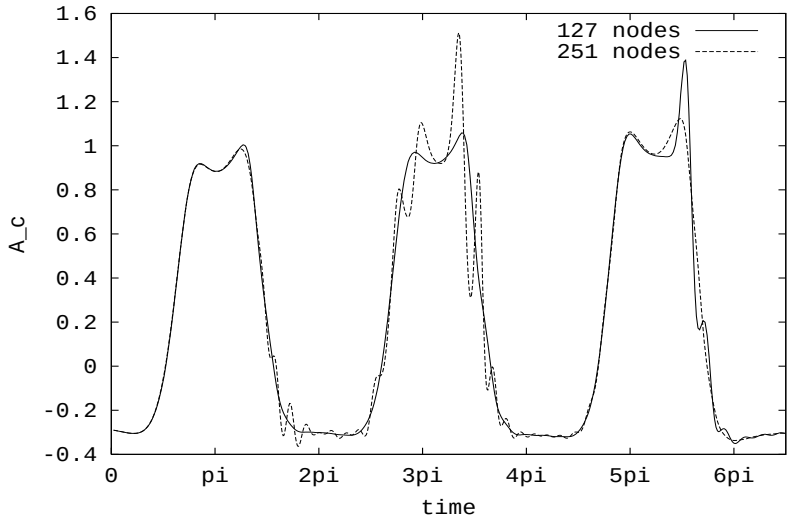

Fig. 9. Evolution of the amplitude of the crest acceleration normalized by the gravitational acceleration (A_c). The case with 127 nodes and 251 nodes on the free surface are shown, respectively. In each case, regridding was used.

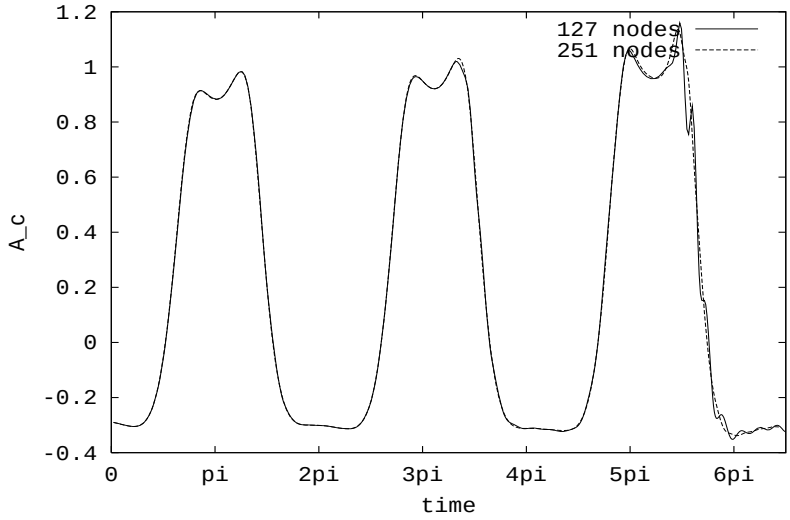

Fig. 10. Evolution of the amplitude of the crest acceleration normalized by gravitational acceleration (A_c). The case with 127 nodes and 251 nodes on the free surface are shown, respectively. In each case, regridding was not used.

Fig. 10 shows the evolution of A_c without using regridding. Two cases are shown. Namely, the case when 127 nodes and 251 nodes were placed on the free surface, respectively. The results for both cases are close, and the disturbances seen in Fig. 9 have diminished.

As a result, in order to simulate the limit LASW, we recommend that regridding should not be used. Spline interpolation in the regridding procedure might be causing the disturbances.

5 The RIG method

If we want to simulate not only standing waves but more general waves like transient waves, regridding may be required. But regridding with simple spline interpolation gives rise to numerical error.

In this part, we propose a method called "RIG" in order to make the wave simulation more accurate. The idea is based on [9][12]. The basic idea is as follows. First, the velocity potential is expanded using the basic functions which satisfy the Laplace's equation. Then, these coefficients are corrected to satisfy Bernoulli's equation rigorously.

5.1 The RIG algorithm

The position of the node i on the free surface is $(x_i, y_i)^{\mathrm{T}}$, and the velocity potential of the node i is ϕ_i. The number of nodes on the free surface is f. The following algorithm gives the time evolution from t to $t + \Delta t$.

Assume that at time t, x_i, y_i, ϕ_i $(i = 1, 2, \ldots, f)$ satisfy Bernoulli's equation (8) rigorously.

(1) Using a time evolution scheme such as in 3.1, compute x_i, y_i, ϕ_i $(i = 1, 2, \ldots, f)$ at $t + \Delta t$.

(2) Regrid the free surface so that x_i remains the same for each node i $(i = 1, 2, \ldots, f)$. Update y_i and ϕ_i $(i = 1, 2, \ldots, f)$ using interpolation.

(3) Using the expansion of the velocity potential [4][12]:

$$\phi(x, y) = \sum_{k=0}^{k_{\max}-1} A_k \frac{\cosh k(y + h)}{\cosh(kh)} \cos(kx), \tag{17}$$

where $k_{\max}$ is the truncation number of the summation and A_k $(k = 0, 1, \ldots, k_{\max-1})$ are the coefficients of the expansion, determine A_k $(k = 0, 1, \ldots, k_{\max-1})$ from x_i, y_i, ϕ_i, $(i = 1, 2, \ldots, f)$ using the least square method. The appropriate value for $k_{\max}$ requires trial and error. Here, we set it to $\left\lfloor \dfrac{f+1}{2} \right\rfloor$. The expansion (17) is derived from the Laplace's equation: $\Delta\phi = 0$ and the bottom and wall boundary conditions: $\dfrac{\partial \phi}{\partial n} = 0$.

(4) Execute the convergence computation with respect to y_i $(i = 1, 2, \ldots, f)$ using the Newton method and Bernoulli's equation as follows.

for $i = 1$ **to** f

while y_i converges **do**

$$y_i \leftarrow y_i - \frac{\phi_t + \frac{1}{2}(\phi_x^2 + \phi_y^2) + gy}{\phi_{ty} + \phi_x\phi_{xy} - \phi_y\phi_{xx} + g}$$

In order to calculate ϕ_t, the time derivative of A_k $(k = 0, 1, \ldots, k_{\max-1})$ are required. To calculate the time derivative of A_k, we must store the A_k $(k = 0, 1, \ldots, k_{\max-1})$ of the previous time steps, and approximate as follows,

$$\frac{\mathrm{d}A_k}{\mathrm{d}t} \approx \frac{11A_k^t - 18A_k^{t-\Delta t} + 9A_k^{t-2\Delta t} - 2A_k^{t-3\Delta t}}{6\Delta t}. \tag{18}$$

(5) When y_i $(i = 1, 2, \ldots, f)$ converge, compute ϕ_i $(i = 1, 2, \ldots, f)$ using Eq. (17).

(6) The free surface should also satisfy the material derivative of Bernoulli's equation,

$$\phi_{tt} + 2\phi_{tx}\phi_x + 2\phi_{ty}\phi_y + 2\phi_{xy}\phi_x\phi_y + \phi_{xx}(\phi_x^2 - \phi_y^2) + g\phi_y = 0. \tag{19}$$

In order to compute Eq. (19), $\dfrac{\mathrm{d}^2A_k}{\mathrm{d}t^2}$ is approximated by

$$\frac{\mathrm{d}^2A_k}{\mathrm{d}t^2} \approx \frac{2A_k^t - 5A_k^{t-\Delta t} + 4A_k^{t-2\Delta t} - A_k^{t-3\Delta t}}{(\Delta t)^2}. \tag{20}$$

The left hand side of Eq. (19) is written as $DPDT(x_i, y_i, \{A_k\})$ for brevity. This is a function of x_i, y_i and $\{A_k\} = \{A_0, A_1, A_2, \ldots, A_{k_{\max-1}}\}$.

Then, $\{A_k\}$ are determined using Newton's method, so that, for each node $i = 1, 2, \ldots, k_{\max}$, $DPDT$ is sufficiently close to 0. To do so, the Jacobian matrix $J = (J_{ij})$ $(i, j = 1, 2, \ldots, k_{\max})$ is required, where

$$J_{ij} = \frac{\partial(DPDT(x_i, y_i, \{A_k\}))}{\partial A_{j-1}}. \tag{21}$$

Since it is complicating to compute the Jacobian matrix analytically, J_{ij} is approximated by

$$J_{ij} = \frac{DPDT(x_i, y_i, \{A_k\} + \varepsilon) - DPDT(x_i, y_i, \{A_k\})}{\varepsilon}, \tag{22}$$

where $\{A_k\} + \epsilon = \{A_0, \ldots, A_{j-2}, A_{j-1} + \epsilon, A_j, \ldots, A_{k_{\max-1}}\}$ and $\epsilon = 10^{-6}$. Then, execute Newton's method as follows.

until $DPDT$ converges to 0 at every node i

$$\begin{pmatrix} A_0 \\ A_1 \\ \vdots \\ A_{k_{\max}-1} \end{pmatrix} \leftarrow \begin{pmatrix} A_0 \\ A_1 \\ \vdots \\ A_{k_{\max}-1} \end{pmatrix} - J^{-1} \begin{pmatrix} DPDT(x_1, y_1, \{A_k\}) \\ DPDT(x_2, y_2, \{A_k\}) \\ \vdots \\ DPDT(x_{k_{\max}}, y_{k_{\max}}, \{A_k\}) \end{pmatrix}$$

When the free surface is symmetric with respect to the y-axis and $k_{\max} = \left\lfloor \frac{f+1}{2} \right\rfloor$, the above Newton's method can be executed.

(7) If the convergence is sufficient in the steps (4) and (6), go to the step (8), otherwise go to step (4).

(8) $t \leftarrow t + \Delta t$.

5.2 Verification of the RIG method

Here, we compare results using RIG with results obtained without RIG. The initial wave profile is given by $\eta(x, 0) = 0.1 \cos x$ with Δt fixed. The time evolution scheme based on Taylor expansion was used.

Fig. 11 shows the fluctuation of the total volume. Four cases are shown. Namely, the case when using RIG with $\Delta t = 0.01$[s] (RIG, dt=0.01), when using RIG with $\Delta t = 0.001$[s] (RIG, dt=0.001), when not using RIG with $\Delta t = 0.01$[s] (noRIG, dt=0.01), and when not using RIG with $\Delta t = 0.001$[s] (noRIG, dt=0.001). 19 nodes were placed on the free surface and 9 nodes on the left and the right wall of the vessel, respectively, and 19 nodes on the bottom line of the vessel. The depth of the vessel is $h = \pi$[m]. It is observed in this figure that when using RIG, the fluctuation of volume is smaller than when RIG was not used.

Similarly, Fig. 12 shows the fluctuation of energy. It is observed that when using RIG, the fluctuation is lager than when RIG was not used. However, when using RIG, the fluctuation has neither an increasing trend nor a decreasing trend.

5.3 Simulation of excited standing waves using RIG

Next, using the RIG method, we will simulate the behavior of standing waves when they are excited in the vertical direction so that the amplitude of the

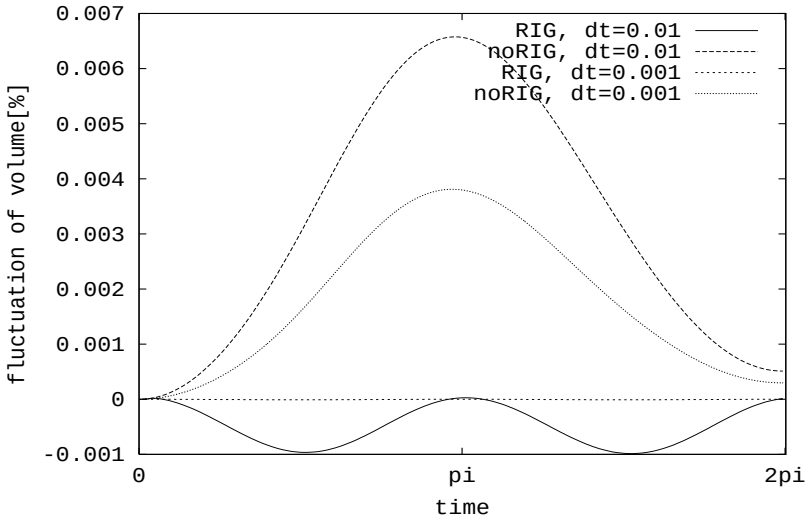

Fig. 11. Evolution of the fluctuation of the volume when the initial amplitude of the free surface is given by $\eta(x,0) = 0.1\cos x$. Four cases are shown: using RIG with $\Delta t = 0.01$[s] (RIG, dt=0.01), using RIG with $\Delta t = 0.001$[s] (RIG, dt=0.001), not using RIG with $\Delta t = 0.01$[s] (noRIG, dt=0.01), and not using RIG with $\Delta t = 0.001$[s] (noRIG, dt=0.001). 19 nodes were placed on the free surface.

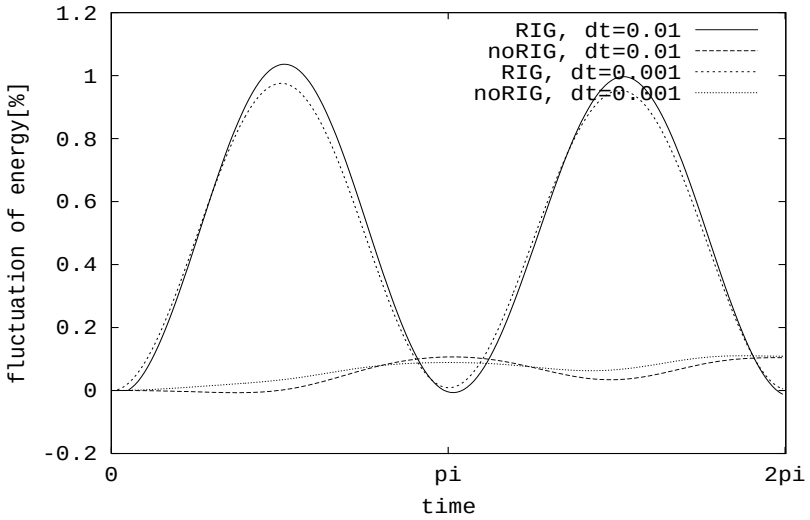

Fig. 12. Evolution of the fluctuation of energy when the initial amplitude of the free surface is given by $\eta(x,0) = 0.1\cos x$. Four cases are shown: using RIG with $\Delta t = 0.01$[s] (RIG, dt=0.01), using RIG with $\Delta t = 0.001$[s] (RIG, dt=0.001), not using RIG with $\Delta t = 0.01$[s] (noRIG, dt=0.01), and not using RIG with $\Delta t = 0.001$[s] (noRIG, dt=0.001). 19 nodes were placed on the free surface.

waves become larger and larger.

The initial wave profile is set to $\eta(x,0) = 0.1\cos x$. The waves are excited intermittently with a period of four seconds. Thus, the commencement of each excitation t_0 is $4j$ ($j = 0, 1, 2, \ldots$). For a example, we excite during

$0 \le t < K,\ 4 \le t < 4+K,\ 8 \le t < 8+K, \ldots$ and we do not excite during $K \le t < 4, 4+K \le t < 8, 8+K \le t < 12, \ldots$.

The gravitational acceleration, which is a function of time $g(t)$, is given by

$$g(t) = \begin{cases} g + d(2\omega)^2 \frac{T^2(T-K)^2}{16} \sin(2\omega T) & (0 \le T < K), \\ g & (K \le T < 4), \end{cases} \tag{23}$$

where $g = 9.8[\mathrm{m/s^2}]$, $|d| = 0.01[\mathrm{m}]$. The sign of d is determined so as not to decrease the energy of the wave. ω is the angular frequency of the free surface, and $K = \dfrac{2\pi}{\omega} \times 2[\mathrm{s}]$. $T = t - t_0$ is the time from the most recent commencement of excitation. $\dfrac{T^2(T-K)^2}{16}$ is introduced for the smooth shifting from the excitation period to the non-excitation period and vice versa.

63 nodes were placed on the free surface and the time evolution scheme based on Taylor expansion was used. Δt was fixed at 0.01[s]. RIG was used.

Fig. 13 shows the evolution of $\eta(0,t)$. It is observed that the simulation fails before $\max\{\eta\} \ge 0.3$ [m]. In the RIG algorithm, higher order approximations:

$$\frac{\mathrm{d}A_k}{\mathrm{d}t} \approx \frac{137A_k^t - 300A_k^{t-\Delta t} + 300A_k^{t-2\Delta t} - 200A_k^{t-3\Delta t} + 75A_k^{t-4\Delta t} - 12A_k^{t-5\Delta t}}{60\Delta t}, \tag{24}$$

$$\frac{\mathrm{d}^2A_k}{\mathrm{d}t^2} \approx \frac{45A_k^t - 154A_k^{t-\Delta t} + 214A_k^{t-2\Delta t} - 156A_k^{t-3\Delta t} + 61A_k^{t-4\Delta t} - 10A_k^{t-5\Delta t}}{12(\Delta t)^2}, \tag{25}$$

were used instead of Eqs. (18), (20) in order to obtain better results.

The reason why the simulation fails might be due to the inaccuracy of the approximation of time derivatives of the velocity potential ϕ_t, ϕ_{ty}, etc.

6 Simulation of large amplitude cosine wave

Using the simulation method of this paper, transient standing waves can be simulated. For example, the large amplitude cosine wave is simulated in this section. The initial wave profile is given by $\eta(x,0) = -0.5\cos x$. No excitation is applied. Discontinuous elements were used at the wall-free surface interface in BEM. The time evolution scheme based on Taylor expansion was used. RIG was not used. 59 nodes were placed on the free surface, and regridding was not used.

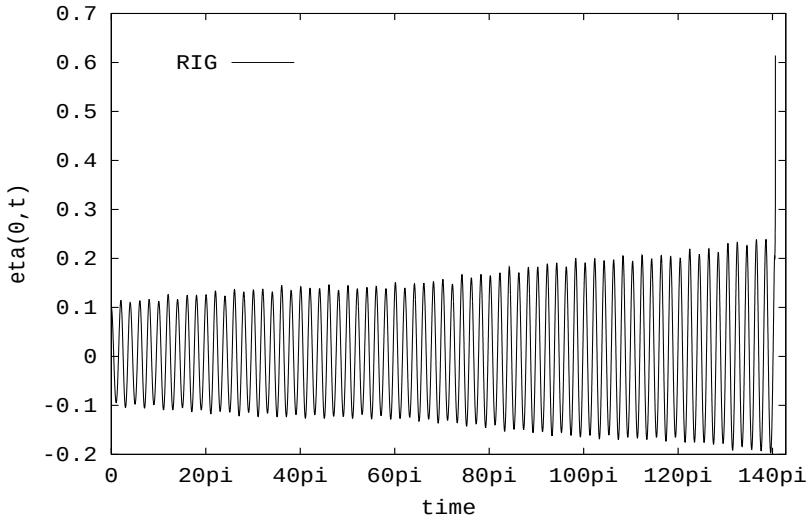

Fig. 13. Evolution of $\eta(0,t)$ for the case when the initial amplitude of the free surface is set to $\eta(x,0) = 0.1\cos x$ and RIG is used. The rectangular vessel is excited intermittently in the vertical direction.

Fig. 14 shows the wave profile at t =0, 0.0659, 0.352, 0.414, 0.486, 0.589 [s], from top to bottom, and then left to right, respectively. Fig. 15 shows the wave profile at t =0.786, 1.07, 1.38, 1.65, 1.92, 2.10 [s], from top to bottom, and then left to right, respectively. The last figure of Fig. 15 shows that the free surface has a very sharp profile. Therefore, we cannot simulate beyond this point. In this case, regridding along the free surface may be necessary.

7 Conclusions

In this paper, large amplitude standing waves (LASW) in a vessel were simulated directly using the boundary element method (BEM). In the simulation, two problems occurred. The first problem was that when double nodes were used at corner nodes where the free surface meets the walls of the vessel, the total energy tended to increase gradually. The second problem was that when not using regridding, projection-like profiles appeared at the end of the free surface which caused the simulation to break down.

The following methods were proposed to overcome these problems. By using discontinuous boundary elements at the corner nodes, the gradual increase of the energy was avoided. By setting the initial wave profile so that the lowest point was at the middle and the highest point at the ends of the free surface, the nodes on the free surface did not concentrate at the ends of the free surface, whereas when the initial wave profile has the lowest point at the ends of the free surface and the highest point at the middle of the free surface, the nodes on the free surface concentrated at the ends of the free surface causing

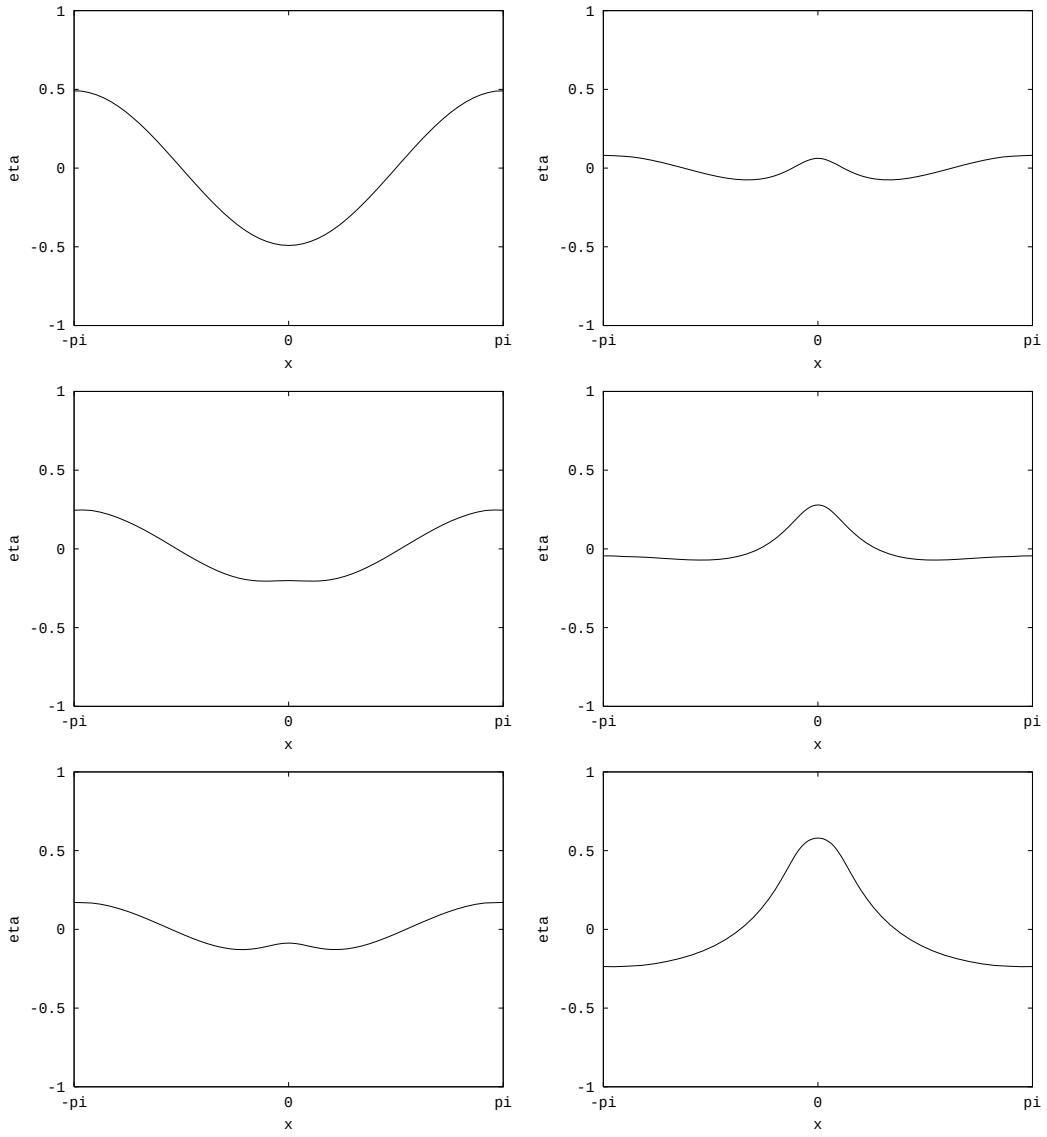

Fig. 14. Time evolution of the free surface from top to bottom, and then left to right. The initial amplitude of the free surface is given by $\eta(x, 0) = -0.5 \cos x$.

projection-like profiles and the simulation to break down.

Hence, the treatment of corner nodes where the free surface meets the vessel is very significant for the stable simulation of LASW.

Simulating without regridding is important when simulating limit amplitude standing waves. However, for situations where regridding is required, we proposed the simulation method RIG, for simulating the free surface with high accuracy. However, RIG still has some problems when simulating LASW. In order to investigate this problem of RIG, validated computation using interval arithmetic may be required.

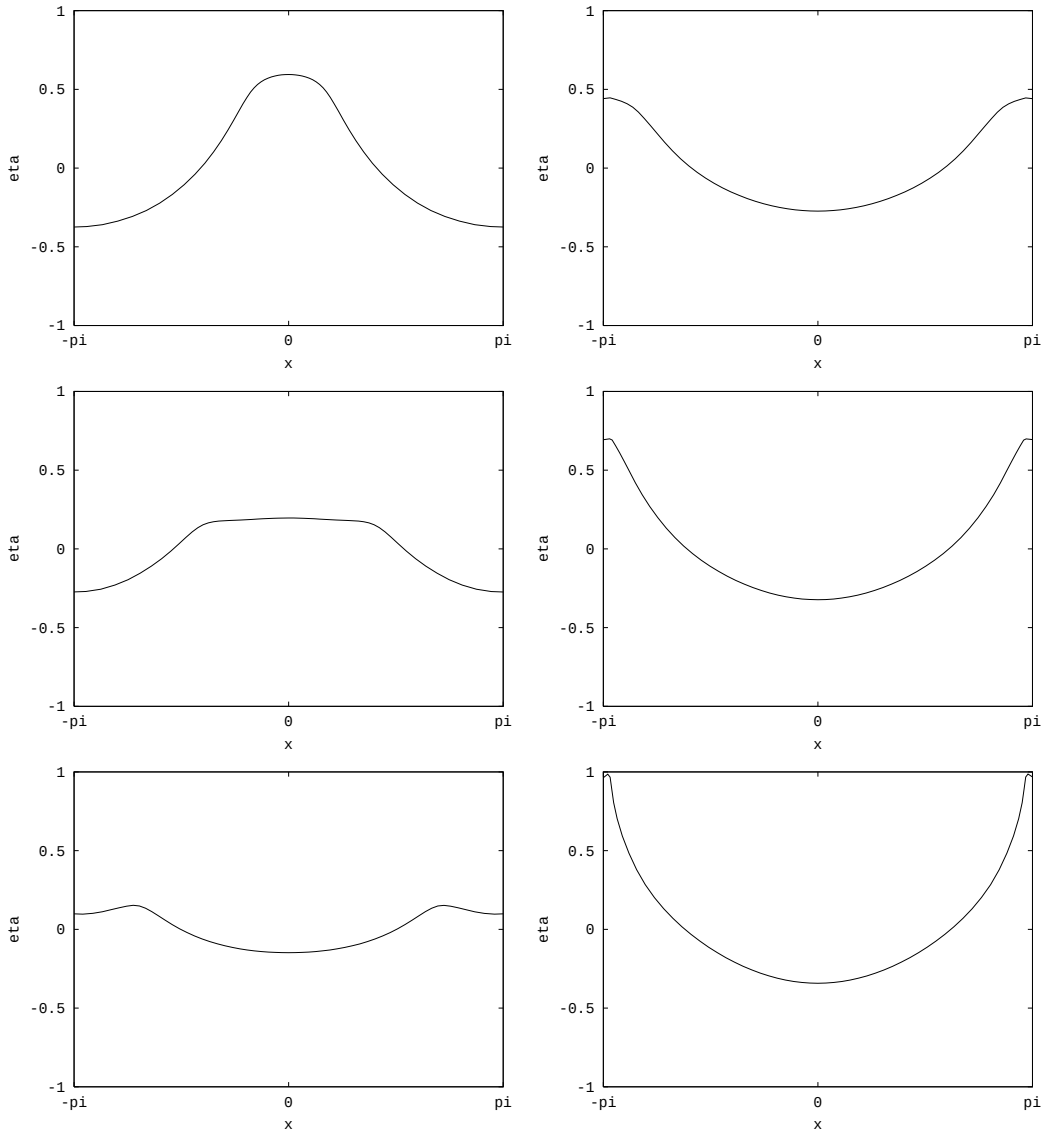

Fig. 15. Time evolution of the free surface from top to bottom, and then left to right. The initial amplitude of the free surface is given by $\eta(x, 0) = -0.5 \cos x$.

Finally, the large amplitude cosine wave was simulated without regridding.

Acknowledgements

We are very grateful to Dr. M. Okamura of Kyushu University, for providing his data on large amplitude stationary standing wave profiles, which were necessary for the initial wave profiles in this paper.

We thank Dr. T. Nakayama of Chuo University, for his detailed explanation of the time evolution scheme based on Taylor expansion.

We also thank Dr. K. Abe of Niigata University, for his enlightening advice and discussions.

References

[1] Benjamin TB, Ursell F. The stability of the plane free surface of a liquid in vertical periodic motion. Proc R Soc Lond 1954;A255:505–515.

[2] Brebbia CA, Dominguez J. Boundary Elements: An Introductory Course. Boston: Computational Mechanics Publications, 1992.

[3] Enokizono M. Boundary Element Analysis (in Japanese). Tokyo: Baifukan, 1986.

[4] Hammack JL. A note on tsunamis: their generation and propagation in an ocean of uniform depth. J Fluid Mech 1973;60(4):769–799.

[5] Hartmann F. Introduction to Boundary Elements: Theory and Applications. Berlin Heidelberg: Springer-Verlag, 1989.

[6] Longuet-Higgins MS, Cokelet ED. The deformation of steep surface waves on water: I. A numerical method of computation. Proc R Soc Lond 1976;A350:1–26.

[7] McLachlan NW. Theory and application of Mathieu functions. London: Oxford University Press, 1947.

[8] Nakayama T. A computational method for simulating transient motions of an incompressible inviscid fluid with a free surface. Int J Numer Meth Fluids 1990;10:683–695.

[9] Okamura M. The profile of large amplitude standing waves (in Japanese). RIMS Kokyuroku 1997;993:134–143.

[10] Press WH, Flannery BP, Teukolsky SA, Vetterling WT. Numerical Recipes in C. Cambridge: Cambridge University Press, 1993.

[11] Saffman PG, Yuen HC. A note on numerical computations of large amplitude standing waves. J Fluid Mech 1979;95(4):707–715.

[12] Tsai CP, Jeng DS. Numerical Fourier solutions of standing waves in finite water depth. Applied Ocean Research 1994;16:185–193.

[13] Wright J, Yon S, Pozrikidis C. Numerical studies of two-dimensional Faraday oscillations of inviscid fluids. J Fluid Mech 2000;402:1–32.